IEEE Access
Multidisciplinary | Rapid Review | Open Access Journal

Received 18 November 2022, accepted 15 December 2022, date of publication 19 December 2022,
date of current version 25 January 2023.

Digital Object Identifier 10.1109/ACCESS.2022.3230907

RESEARCH ARTICLE

Analysis of Stator Vibration Characteristics in Synchronous Generators Considering Inclined Static Air Gap Eccentricity

YU-LING HE[1], (Senior Member, IEEE), YONG LI[1], (Graduate Student Member, IEEE), WEN ZHANG[1], (Graduate Student Member, IEEE), MING-XING XU[1], (Graduate Student Member, IEEE), YI-FAN BAI[1], (Student Member, IEEE), XIAO-LONG WANG[1], (Member, IEEE), SHAN-ZHE SHI[2], AND DAVID GERADA[3], (Senior Member, IEEE)

[1]Hebei Key Laboratory of Electric Machinery Health Maintenance and Failure Prevention, North China Electric Power University, Baoding 071003, China
[2]State Grid Hebei Electric Power Company, Shijiazhuang 050022, China
[3]Department of Electrical and Electronics Engineering, University of Nottingham, NG7 2RD Nottingham, U.K.

Corresponding author: Xiao-Long Wang (wangxiaolong0312@126.com)

This work was supported in part by the National Natural Science Foundation of China under Grant 51777074 and Grant 52177042, in part by the National Natural Science Foundation of Hebei Province under Grant E2020502032, in part by the Chinese Fundamental Research Funds for the Central Universities under Grant 2020MS114, in part by the Top Youth Talent Support Program of Hebei Province under Grant [2018]-27, and in part by the Suzhou Social Developing Innovation Project of Science and Technology under Grant SS202134.

ABSTRACT This paper mainly focuses on the impact of inclined static air gap eccentricity (ISAGE) on the electromagnetic characteristics and mechanical performances (vibration, deformation, strain and stress). Considering different ISAGE fault types in the theoretical and finite element analysis (FEA) model of synchronous generators, the effects of intersection position of the rotor center axis and stator center axis, rotor inclined angle, and the combination of the previous two fault types on MFD, phase current and radial magnetic pulling per unit area (MPPUA) are analyzed and compared. Then, based on the stator model used uniformly in three physical fields, the harmonic response and mechanical response are investigated with loads imported by the electromagnetic field. Finally, the stator radial vibration measurement experiments are carried out to verify the results obtained by theoretical analysis and FEA. It is shown that ISAGE will considerably enlarge the fluctuation of MPPUA and intensify the radial vibration of the stator, especially at the 2nd harmonic. The probability of failure at tooth tip and inner slot wall of the stator will increase.

INDEX TERMS Synchronous generator, inclined static air gap eccentricity, magnetic pulling force per unit area, stator vibration.

I. INTRODUCTION

The air gap length between the rotor and the stator is difficult to maintain uniformly in the generator/motor, which will lead to air gap eccentricity faults [1], [2]. Generally, scholars divide the air gap eccentricity into static air gap eccentricity (SAGE), dynamic air gap eccentricity (DAGE) and hybrid air gap eccentricity (HAGE) [3], [4], respectively, depending on whether the minimum position of the air gap length changes with the rotation of the rotor. The conventional air gap eccentricity assumes that one side is larger and the other side is smaller, and the eccentricity is uniformly distributed along the generator/motor axial direction. However, it is hard to keep the central axis of the stator and the rotor aligned at all times. As a result, it will lead to a change of air gap eccentricity along the axial direction, which is known as inclined eccentricity fault [5], as seen in Fig.1 (b)-(d). Furthermore, inclined eccentric faults can be divided into inclined static air gap eccentricity and inclined dynamic air gap eccentricity. As for inclined static air gap eccentricity

The associate editor coordinating the review of this manuscript and approving it for publication was Mehrdad Saif.

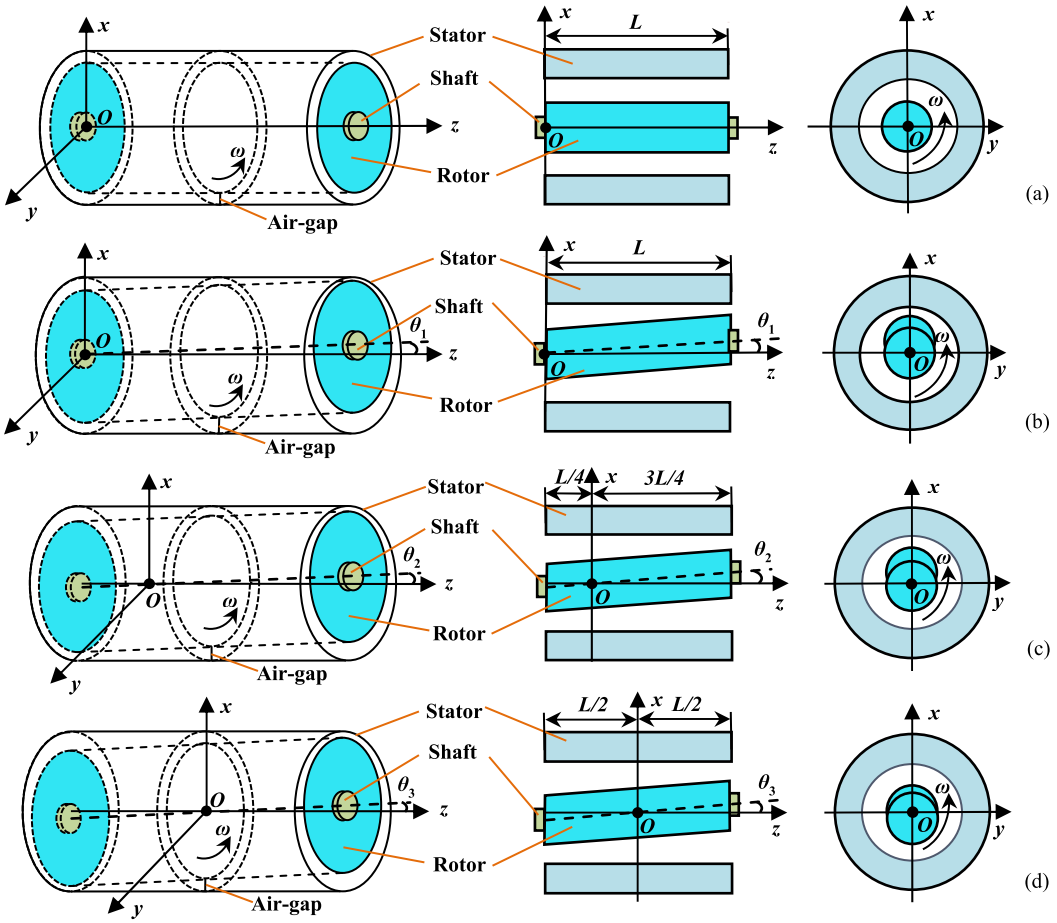

FIGURE 1. Physical model of generator, (a) normal case, (b) ISAGE-1 case, (c) ISAGE-2 case, (d) ISAGE-3 case.

(ISAGE), the central axis of the rotor coincides with the axis of rotation, as shown in Fig.1 (b)-(d). Whereas, for inclined dynamic air gap eccentricity (IDAGE), the rotor rotation axis overlaps with the central axis of the stator. More importantly, the minimum air gap length along the radial direction will be changed in IDAGE but not in ISAGE.

Due to the manufacturing error [6] and bearing wear [7], the SAGE fault will be induced and aggravated. Consequently, it will impair the generator's operation. For instance, the unbalanced magnetic pull (UMP) will affect the stator and rotor when SAGE happens [8]. More seriously, the stator deformation [9] and stator vibration [10] will increase with the development of SAGE degrees, and even break down the insulation of the stator winding [11]. When compared to the DAGE, the SAGE causes more eccentricity, which has a greater effect on generators. When the SAGE degree reaches 10% [12], the generator must be repaired to avoid deterioration of the faults.

Scholars are currently investigating the SAGE fault, focusing primarily on radial SAGE. For example, the double fundamental frequency of rotor current will be raised [13]. The radial SAGE will intensify the electromagnetic torque ripple (EMT) and increase each harmonic of EMT [14]. In addition, the mechanical stress will be worsened by radial SAGE [15]. The occurrence of SAGE will significantly increase the electromagnetic forces and the vibration amplitudes on some coils [16]. I. R. Ciric proposed an efficient iterative integral technique to investigate the rotor eccentricity impact on MFD [17]. What's more, Y. He studied the combined fault (SAGE and stator inter-turn short circuit [18], [19], SAGE and rotor inter-turn short circuit [20]) and found that SAGE will not only enlarge the amplitude of the MFD [18], but also increase the core loss of the stator and rotor [19], [20]. Apart from the analysis of electromechanical characteristics in SAGE fault analysis, scholars also developed the diagnostic method to monitor the SAGE fault. For example, G. Mirzaeva presents a new technique for early detection of rotor bar faults and mixed eccentricity based on the models of MFD [21]. Compared to the installation of additional monitor components inside generators, the vibration signal of the stator and rotor for diagnosing SAGE will be more convenient [22], [23], [24].

In fact, most studies target the SAGE fault in a radial section or assume that the eccentricity is evenly distributed along the axis. However, the radial SAGE usually changes with the generator axis. Therefore, ISAGE is widely present in generators when radial SAGE happens. As early as 1992, Y. Akiyama found that the eccentricity would be unevenly dis-

tributed along the axial direction, and proposed the concept of ISAGE [25]. After that, scholars carried out lots of research on ISAGE. M. Ojaghi [26] presented a modified 2-D winding function theory that can be used to analyze SCIM performance under ISAGE faults as well as the healthy condition. During ISAGE, D. G. Dorrell [27] calculated the rotor UMP and verified it with ten- and four-pole machines. Moreover, the electromagnetic forces acting between the rotor and stator when the rigid rotor is performing ISAGE are studied [28]. X. Li found that the current spectrum could not detect the degree of inclined eccentricity, and the vibration signal for ISAGE monitoring will be a better choice [29]. Comparing rotor vibration with stator vibration, the former will have an impact on bearing failures [30]. However, the stator vibration has less influence from the outside. On the other hand, there is little research on stator vibration in the ISAGE fault. In this case, the investigation of stator vibration characteristics with ISAGE will benefit the generator condition monitor.

In this paper, we propose a comprehensive study of the stator vibration characteristics of generators under ISAGE, which will be an important supplement to the monitoring and diagnosis of generators. The rest of this paper is arranged as follows. Section 2 presents a theoretical analysis model in detail. Then section 3 verifies the model by finite element calculation and experimental tests on a two-pole prototype generator. Section 4 summarizes the conclusions.

II. THEORETICAL MODEL

A. PHYSICAL MODEL OF ISAGE

The central axis of the rotor and stator coincide with each other in an ideal normal condition, as shown in Fig. 1 (a). The conventional radial SAGE assumes that the whole rotor is moved in the radial direction. However, the degree of bearing wear on both sides of the rotor is not uniform, which will lead to ISAGE. The rotor center axis will be inclined at a certain angle and intersect with the stator center axis at a point in the ISAGE case, as indicated in Fig. 1 (b)-(d).

This intersection point is specified as the coordinate origin (o) when establishing the 3D cartesian coordinate system. Particularly, the intersection points of different ISAGE cases are inconsistent. In order to analysis the ISAGE fault as closely as possible, this paper proposes three typical cases. In case 1, the intersection point is located at the far left of the stator axis, named ISAGE-1, as indicated in Fig. 1 (b). In case 2, the intersection point is located at the left quarter position of the stator axis, named ISAGE-2, as indicated in Fig. 1 (c). In case 3, the intersection point is located at the midpoint of the stator axis, named ISAGE-3, as indicated in Fig. 1 (d). Theoretically, the point of intersection could also continue to move to the right of the midpoint of the stator axis, but due to the symmetry of the rotor, this would repeat the previous case from ISAGE-1 to ISAGE-3. For example, when the intersection point is at the far right of the stator axis, its structure can be completely consistent with ISAGE-1 after the whole rotation, which is repeated with ISAGE-1. Meanwhile, the inclined angle (θ) will also impact the ISAGE fault, as shown in Fig. 1 (b)-(d).

B. IMPACT OF ISAGE ON MFD

The air MFD can be obtained by multiplying magnetomotive force (MMF) with permeance per unit area (PPUA). Generally, PPUA can be written as

$$\Lambda\left(\alpha_m, z, \theta\right) = \frac{\mu_0}{g\left(\alpha_m, z, \theta\right)} \tag{1}$$

where μ_0 is the permeability of air, g is the radial length of the air gap, α_m is the mechanical angle used to indicate the circumferential position of the air gap, z is the z-coordinate value of the radial section in the 3D cartesian coordinate system, θ is the inclination angle of the rotor.

According to Eq. (1), the PPUA will be influenced by the radial air gap length. As seen in Fig. 2 (a), the radial air gap length is evenly distributed in an ideally normal condition. In addition, the air gap length distribution in radial section is shown in Fig. 2 (b).

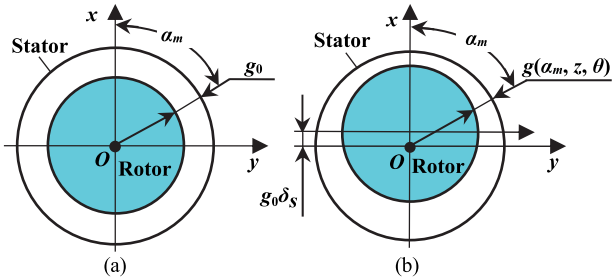

FIGURE 2. Air gap length in radial section view, (a) normal case, (b) ISAGE case.

The radial air gap length changes along the z axis direction when ISAGE occurs, as seen in Fig.1 (b)-(d). The radial eccentricity along the z axis direction can be written as

$$g_0\delta_s = \begin{cases} 0 \cdots\cdots\cdots\cdots\cdots\cdots\cdots\cdots \text{Normal} \\ z\tan\theta, \quad z \in [0, L] \cdots\cdots\cdots \text{ISAGE-1} \\ z\tan\theta, \quad z \in \left[-\frac{1}{4}L, \frac{3}{4}L\right] \cdots \text{ISAGE-2} \\ z\tan\theta, \quad z \in \left[-\frac{1}{2}L, \frac{1}{2}L\right] \cdots \text{ISAGE-3} \end{cases} \tag{2}$$

where g_0 is the average length of the radial air gap in normal condition, δ_s is the relative degree of eccentricity, L is the stator length of the generator.

In particular, from cases ISAGE-1 to ISAGE-3, the z-coordinate value corresponding to the radial section of the generator will change as the origin of the coordinates gradually approaches the midpoint of the stator center axis, as seen in Fig.1 (b)-(d). Specifically, a 2-pole prototype generator with a stator length of 130mm is taken as an example to illustrate. When the radial section is located at 97.5 mm (3/4L) to the right side of the left end face of the stator, the corresponding z-coordinate values of cases ISAGE-1 to ISAGE-3 are 3/4L, 1/2L, and 1/4L, respectively, and the ratio of radial eccentricity $g_0\delta_s$ calculated according to Eq. (2)

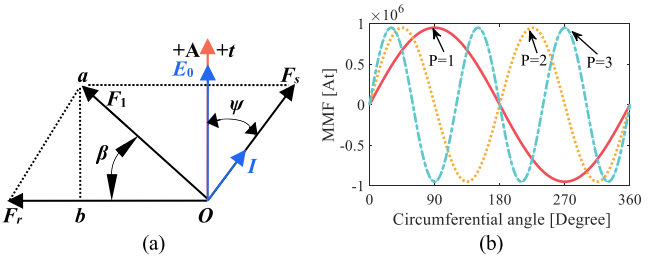

FIGURE 3. Diagram of MMF in normal and ISAGE cases, (a) diagram of MMF vectors, (b) The spatial distribution of MMF under P=1-3.

is 3:2:1, so this radial section can be used for subsequent comparative analysis.

Affected by the air gap length, the rotor maximum inclination angle can be expressed as

$$\theta_{\max} = arctg\frac{g_0}{z_{\max}} = \begin{cases} arctg\dfrac{g_0}{L} \cdots \text{ISAGE-1} \\ arctg\dfrac{4g_0}{3L} \cdots \text{ISAGE-2} \\ arctg\dfrac{2g_0}{L} \cdots \text{ISAGE-3} \end{cases} \tag{3}$$

where $z_{\max}$ is the maximum value of the z-coordinate in each ISAGE case.

For this paper, a generator with a stator axial length of 130mm and an air gap length of 1.2mm is used for analysis object, the corresponding maximum inclination angles of cases ISAGE-1 to ISAGE-3 are 0.53°, 0.71°, and 1.06°, respectively. It is worth noting that when the inclination angle reaches its maximum value, the rotor and the stator have already made contact, which will cause serious damage to the generator. Literature [12] points out that the maximum eccentricity of the generator cannot exceed 10%. Therefore, when the inclination angle of the rotor reaches 10% of the maximum value in each case, the generator must be repaired to avoid further deterioration of the fault.

The radial air gap length can be written as

$$g(\alpha_m, z, \theta) = \begin{cases} g_0 \cdots \text{Normal} \\ g_0\left(1 - \dfrac{z\tan\theta}{g_0}\cos\alpha_m\right) \cdots \text{ISAGE} \end{cases} \tag{4}$$

Feeding Eq. (4) into Eq. (1), the PPUA in the ISAGE case is obtained through the expansion of the Maclaurin series, and ignoring the Peano remainder, the PPUA can be written as (5), shown at the bottom of the page, where the Λ_0 is the constant value of PPUA.

Similar to SAGE, ISAGE further affects MFD by affecting PPUA, while having little impact on MMF [18], as shown in Fig. 3 (a). Ideally, integer slot motors/generators only contain integer harmonics, neglecting the higher harmonics, the MMFs can be written as

$$\begin{aligned} f(\alpha_m, t) &= F_r\cos(\omega t - p\alpha_m) \\ &\quad + F_s\cos(\omega t - p\alpha_m - \psi - \pi/2) \\ &= F_1\cos(\omega t - p\alpha_m \\ &\quad - \beta) \cdots \cdots \cdots \cdots \text{Normal/ISAGE} \end{aligned} \tag{6}$$

where

$$\begin{cases} F_1 = \sqrt{F_s^2 + F_r^2 - 2F_sF_r\sin\psi} \\ \beta = arctg\dfrac{F_s\cos\psi}{F_r - F_s\sin\psi} \end{cases} \tag{7}$$

where F_s and F_r are the stator MMF and the rotor MMF, respectively, p is the number of pole pairs, ψ is the internal power angle of the generator, and β is the angle between the composite MMF F_1 and the rotor MMF F_r in normal or ISAGE. Besides, we also show the impact of p on the composite MMF based on Eq. (7), as seen in Fig. 3 (b).

Then, the MFD can be expressed as (8), shown at the bottom of the next page.

Eq. (8) shows that the ISAGE fault mainly increases the fundamental frequency time harmonics of the MFD. However, ISAGE also affects the spatial harmonics of MFD, which can be further expressed as (9), shown at the bottom of the next page.

It can be seen that MFD only includes p-order spatial harmonics under normal case. However, in the case of the ISAGE fault, MFD has new harmonics of ($p\pm1$) and ($p\pm2$) order, but p-order spatial harmonics still dominate. According to Eq. (9), the MFD in ISAGE is affected by both z and θ. Taking the normal case as a reference, the larger the θ is, the greater the change in the amplitude of the MFD's fundamental frequency will be. On the other hand, the closer the radial section of the generator is to the right end face of the stator ($z\uparrow$), the greater the variation of MFD fundamental frequency amplitude will be.

As mentioned before, a 2-pole prototype generator with a stator axial length of 130 mm is used as an example in this paper. Its 3D MFD is plotted according to the theoretical formula in each case when the inclination angle (θ) is 0.04°, as shown in Fig. 4. In order to clearly show the change rule of MFD in the z-axis direction, various colours are used to

$$\Lambda(\alpha_m, z, \theta) = \begin{cases} \dfrac{\mu_0}{g_0} = \Lambda_0 \cdots \cdots \cdots \cdots \cdots \cdots \cdots \cdots \cdots \cdots \cdots \cdots \cdots \cdots \cdots \cdots \text{Normal} \\ \Lambda_0\left[1 + \dfrac{z\tan\theta}{g_0}\cos\alpha_m + \dfrac{z^2\tan^2\theta}{g_0^2}\cos^2\alpha_m + o\left(\dfrac{z^2tan^2\theta}{g_0^2}\cos^2\alpha_m\right)\right] \\ \approx \Lambda_0\left[1 + \dfrac{z\tan\theta}{g_0}\cos\alpha_m + \dfrac{z^2\tan^2\theta}{2g_0^2}(1 + \cos 2\alpha_m)\right] \cdots \text{ISAGE} \end{cases} \tag{5}$$

represent the z-axis coordinate values and projected to the bottom surface. It can be seen that the MFD along the axial orientation is immutable with an evenly distributed air gap of in normal conditions, which is indicated in Fig. 4 (a). It is worth noting that although the 3D MFD of different cases has a similar trend of change along the z–axis ($z\uparrow$, MFD$\uparrow$) when the inclination angle (θ) is constant in the case of ISAGE, there are differences in the magnitude of the change, as shown in Fig. 4 (b)-(d). Specifically, the coordinate systems corresponding to each case are different, and the z-axis coordinate values corresponding to the radial section at the same position of the generator are also different. The closer the origin point (o) is to the midpoint of the stator center axis, the smaller the z-axis coordinate value corresponding to the radial section ($z\downarrow$) and the smaller the MFD fundamental frequency amplitude of the radial section will be. Therefore, among the three cases, the ISAGE-3 case has the smallest MFD amplitude. From another point of view, due to the variation of the coordinate origin (o), the maximum value of $g_0\delta_s$ in ISAGE-1 is four-thirds of ISAGE-2 and twice of ISAGE-3, as seen in Fig. 1 (b)-(d). Therefore, the MFD's fundamental frequency amplitude of ISAGE-1 has the largest change, as shown in Fig. 4 (b).

The inclination angle (θ) also influences the MFD in ISAGE. Similarly, the difference in inclination angle only affects the change amplitude, and the overall change trend of 3D MFD is consistent ($\theta\uparrow$, MFD$\uparrow$). Since it is difficult to compare 3D MFDs with different inclination angles when they are displayed alone, a radial section is selected to compare the MFDs of each case. In this paper, the radial section at 97.5mm (3/4L) on the right side of the left end face of the stator is selected. The reason is that according to Eq. (2), the ratio of radial eccentricity $g_0\delta_s$ in this radial section for cases ISAGE-1 to ISAGE-3 is 3:2:1. Taking ISAGE-2 as an example for analysis, the inclination angles are 0.02°, 0.04°, and 0.06°, respectively. The MFD theoretical curve is shown in Fig.5. It can be seen that the amount of fundamental frequency amplitude variation of the MFD is positively correlated with the inclination angle.

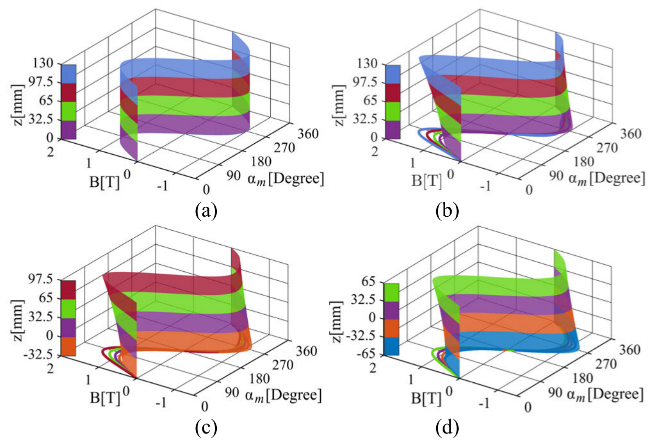

FIGURE 4. Influence of different cases on theoretical 3D MFD, (a) normal, (b) ISAGE-1 case when θ is 0.04°, (c) ISAGE-2 case when θ is 0.04°, (d) ISAGE-3 case when θ is 0.04°.

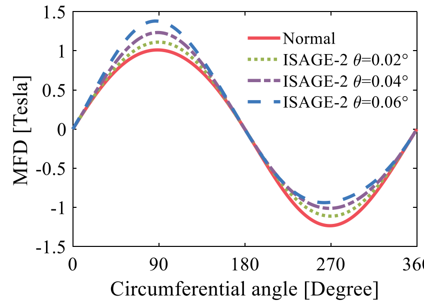

FIGURE 5. Influence of inclination angle on theoretical MFD in ISAGE-2 cases.

C. MPPUA BEFORE AND AFTER ISAGE

The structure of the generator stator is a hollow shell, and its rigidity in the radial direction is lower than axial direction,

$$B(\alpha_m, z, \theta, t) = f(\alpha_m, t)\,\Lambda(\alpha_m, z, \theta) = \begin{cases} F_1\Lambda_0 \cos(\omega t - p\alpha_m - \beta) \cdots\cdots \text{Normal} \\ F_1\Lambda_0\left[1 + \dfrac{z\tan\theta}{g_0}\cos\alpha_m + \dfrac{z^2\tan^2\theta}{2g_0^2}(1+\cos 2\alpha_m)\right]\times \\ \cos(\omega t - p\alpha_m - \beta) \cdots\cdots \text{ISAGE} \end{cases} \tag{8}$$

$$B(\alpha_m, z, \theta, t) = f(\alpha_m, t)\,\Lambda(\alpha_m, z, \theta) = \begin{cases} F_1\Lambda_0\ \cos(p\alpha_m + \beta - \omega t) \cdots\cdots \text{Normal} \\ F_1\Lambda_0\left\{\left(1 + \dfrac{z^2\tan^2\theta}{2g_0^2}\right)\cos(p\alpha_m + \beta - \omega t) + \right. \\ \dfrac{z\tan\theta}{2g_0}\{\cos[(p+1)\alpha_m + \beta - \omega t] + \cos[(p-1)\alpha_m + \beta - \omega t]\} + \\ \left.\dfrac{z^2\tan^2\theta}{4g_0^2}\{\cos[(p+2)\alpha_m + \beta - \omega t] + \cos[(p-2)\alpha_m + \beta - \omega t]\}\right\} \\ \cdots\cdots \text{ISAGE} \end{cases} \tag{9}$$

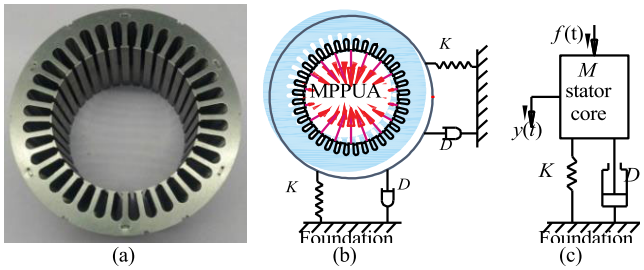

FIGURE 6. Stator core model, (a) real stator core, (b) radial load of stator core, (c) mechanics model of stator core.

as shown in Fig. 6 (a). During the generator operation, the inner circular surface of the stator will be subjected to magnetic pulling per unit area (MPPUA) that is the essential excitation force of the stator vibration response, as indicated in Fig. 6 (b). The mechanical response model of the stator core is illustrated in Fig. 6 (c). According to the relationship between MPPUA and vibration of the stator core, the dynamic equation can be expressed as

$$\begin{cases} [m]\left\{y''(t)\right\} + [D]\left\{y'(t)\right\} + [K]\{y(t)\} = \{f(t)\} \\ a = y''(t) \end{cases} \tag{10}$$

where $[m]$ is the mass matrix of the stator core mass point, $[D]$ is the radial damping matrix, $[K]$ is the radial stiffness matrix. $y(t)$ is the radial displacement of the unit mass point, $y'(t)$ is the radial speed, $y''(t)$ is the radial acceleration and $f(t)$ is the essential excitation force of the stator, which is MPPUA. In addition, MPPUA is difficult to measure directly. In the experiment, acceleration sensors are used for vibration measurement, which reflects radial acceleration.

The resultant of MPPUA acting on the entire stator core is zero in normal conditions, while it has pulsating properties, and the amplitude will change periodically. Acting through the MPPUA, the stator core will undergo contraction-expansion movement at the same frequency as the MPPUA, that is, radial vibration. According to the Maxwell tensor method, the MPPUA can be expressed as [10]

$$\begin{aligned} q\left(\alpha_m, z, \theta, t\right) &= \frac{B^2(\alpha_m, z, \theta, t)}{2\mu_0} = \frac{\left[f\left(\alpha_m, t\right) \Lambda\left(\alpha_m, z, \theta\right)\right]^2}{2\mu_0} \\ &= \frac{f^2\left(\alpha_m, t\right) \mu_0}{2g^2\left(\alpha_m, z, \theta\right)} \end{aligned} \tag{11}$$

TABLE 1. Amplitude formulas and influential factors of MPPUA.

Cases	DC/2nd (N/m^2)	Influential factors	Trend
Normal	$\frac{F_1^2\Lambda_0}{4g_0}$	$I_f, p, z, g_0, \psi,$	--
ISAGE	$\frac{F_1^2\Lambda_0}{4g_0}\left[1+\frac{2ztan\theta}{g_0}cos\alpha_m+\frac{3z^2tan^2\theta}{2g_0^2}\left(1+\cos 2\alpha_m\right)\right]$	$I_f, p, z, g_0, \psi, \theta$	increase

Feed Eq. (4) and Eq. (6) into Eq. (11), Similarly, the MPPUA in the ISAGE case is obtained through the expansion of the Maclaurin series, and ignoring the Peano remainder, the MPPUA can be written as (12), shown at the bottom of the page.

As shown in Eq. (12), the MPPUA can be divided into two parts in normal condition. The first part is the DC component, which is a constant value, it will not cause the stator to vibrate, but it will induce the stator to produce a certain radial deformation in long-term action. The second part is the 2nd harmonic component, which will cause the stator to generate radial vibration at the 2nd harmonic frequency. As for the ISAGE case, the MPPUA also includes two parts. The difference between normal and ISAGE is that each harmonic component of MPPUA in ISAGE fault is larger than former. To explain this phenomenon in detail, the expression of MPPUA amplitude and its influencing factors are sorted out in Table 1, where I_f is the excitation current.

III. FEA AND EXPERIMENT VALIDATION

A. FEA AND EXPERIMENT SETUP

The CS-5 prototype generator in the State Key Laboratory of Alternate Electrical Power Systems with Renewable Energy Sources, P.R. China, is employed as the research object for both the 3D finite element calculation and the experimental verification, as indicated in Fig. 7 (a), its primary parameters are listed in Table 2.

The generator and drive motor are fixed on the bottom steel plate through the bearing seat. Four regulative screws from 1 to 4 for adjusting the horizontal radial movement of the stator are installed at the front and rear of the generator, and the radial movements of the stator are controlled by two dial indicators, as seen in Fig. 7 (b). The ISAGE case can be simulated by adjusting the radial movement of the stator at the front and rear ends, as shown in Fig. 7 (b). During the

$$q\left(\alpha_m, z, \theta, t\right) = \begin{cases} \dfrac{F_1^2\Lambda_0}{4g_0}\left[1+\cos\left(2\omega t - 2p\alpha_m - 2\beta\right)\right] \cdots\cdots\cdots\cdots\cdots\cdots\cdots\cdots \text{Normal} \\ \dfrac{F_1^2\Lambda_0}{4g_0}\left[1+\dfrac{2ztan\theta}{g_0}cos\alpha_m+\dfrac{3z^2tan^2\theta}{g_0^2}\cos^2\alpha_m+o\left(\dfrac{z^2tan^2\theta}{g_0^2}\cos^2\alpha_m\right)\right]\times \\ \left[1+\cos\left(2\omega t - 2p\alpha_m - 2\beta\right)\right] \\ \approx \dfrac{F_1^2\Lambda_0}{4g_0}\left[1+\dfrac{2ztan\theta}{g_0}cos\alpha_m+\dfrac{3z^2tan^2\theta}{2g_0^2}\left(1+\cos 2\alpha_m\right)\right]\times \\ \left[1+\cos\left(2\omega t - 2p\alpha_m - 2\beta\right)\right] \cdots\cdots\cdots\cdots\cdots\cdots\cdots\cdots\cdots\cdots \text{ISAGE} \end{cases} \tag{12}$$

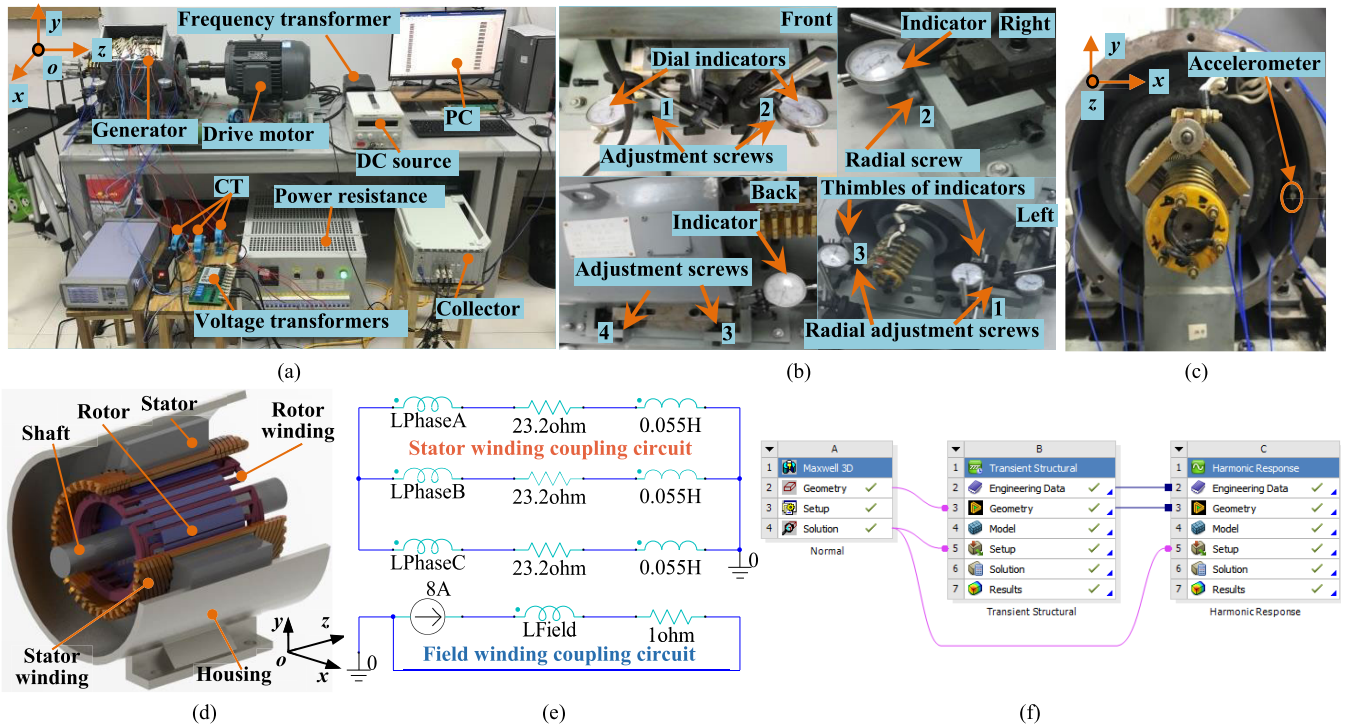

FIGURE 7. CS-5 prototype generator, (a) experiment test rig, (b) method to set ISAGE, (c) vibration sensors, (d) 3D FEA model, (e) external coupling circuit model, (f) electromagnetic- mechanical coupling model.

TABLE 2. Parameters of CS-5 prototype generator.

Parameters	Value	Parameters	Value
Rated Capacity	5 kVA	Rated voltage	380V
Rated rotating speed	3000 r/min	Pole pairs	1
Power factor	cosφ=0.8	Stator slots	36
Radial air gap length	1.2 mm	Pitch distance	14
Stator core length	130 mm	Exciting turns	480
Turns per phase	264	Parallel branches	2

coordinate origin (o) changes and the inclined angle (θ) is a constant simulation, step 1: the screws of No. 1 and No. 4 will keep stationary, while the screws of No. 2 and No. 3 screws will be move for an inclined angle, as seen in Fig. 7 (b). Step 2: the No. 1 to No. 4 screws will be adjusted for stator radial movement, as shown in Fig. 7 (b). Based on step 1 and 2, the ISAGE case with the coordinate origin (o) changing can be achieved by keeping inclined angle (θ) constant. Similarly, in the ISAGE case, with inclined angle (θ) changes when the coordinate origin (o) constant can be achieved by keeping No. 1 and No. 4 stationary, and adjusting No. 2 and No. 3 screws. A tiny PCB acceleration sensor is installed on the stator house to test radial vibration, as shown in Fig. 7 (c).

A 3D generator model is used for the finite element calculation, as indicated in Fig. 7 (d). During FEA, the coordinate origin (o) is consistent with ISAGE model in Fig. 1. Furthermore, the rotor rotates on the XOZ plane with the coordinate origin as the center of rotation, and the rotor inclined angle (θ) are each set to 0.02°, 0.04°, and 0.06°.

During the experiment and FEA, the exciting current was set to 8 A, with 23.2 Ohm of resistance and 0.055 H of inductance connected to each phase, as indicated in Fig. 7 (e). Based on Ansys Workbench software, the electromagnetic results are imported into the structural and harmonic response modules for calculating the deformation, strain, stress and vibration acceleration of the stator in FEA, see Fig. 7 (f). Experiments and FEA are taken 10 times, respectively, as shown in Table 3.

B. FEA RESLUTS AND DISCUSSION

The FEA results with a change coordinate origin (o) when the inclined angle (θ) constant in the ISAGE case is shown in Fig. 8. Taking the value of θ equal to 0.04 as an example, the 3D MFD and its bottom projection of various ISAGE coordinate origin (o) position cases are shown in Fig. 8 (c)-(h). The 3D MFD of the generator remains unchanged in the axial direction in normal condition, as shown in Fig. 8 (a). Comparing Fig. 8 (c)-(d) with Fig. 8 (e)-(f) and Fig. 8 (g)-(h), it can be found that with the increase of the z value, the amount of amplitude variation of the MFD will also be enlarged. Particularly, the ISAGE-1 case has the largest upward movement in axial direction, whereas the ISAGE-3 case has the smallest movement in the axial direction. This result well follows the theoretical analysis.

Generally, for a certain inclined angle, no matter where the point of intersection is, the most severe eccentricity occurs on the ends of the stator or rotor. However, the end section belongs to the limit boundary position in the case and hardly represents most of the sections. According to Eq. (2), radial

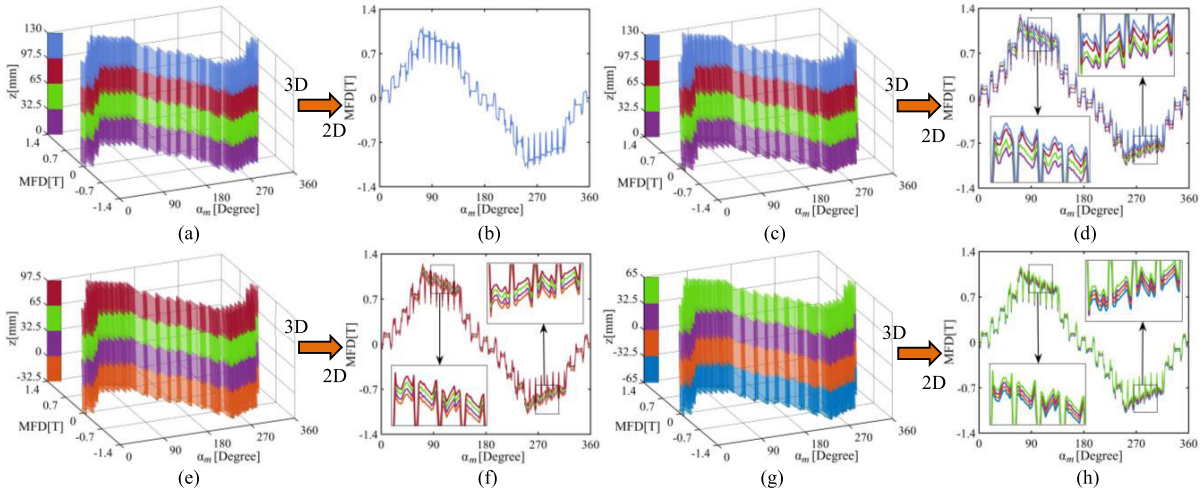

FIGURE 8. 3D MFD and its 2D top view of different cases, (a)-(b) normal case, (c)-(d) ISAGE-1 case when θ is 0.04°, (e)-(f) ISAGE-2 case when θ is 0.04°, (g)-(h) ISAGE-3 case when θ is 0.04°.

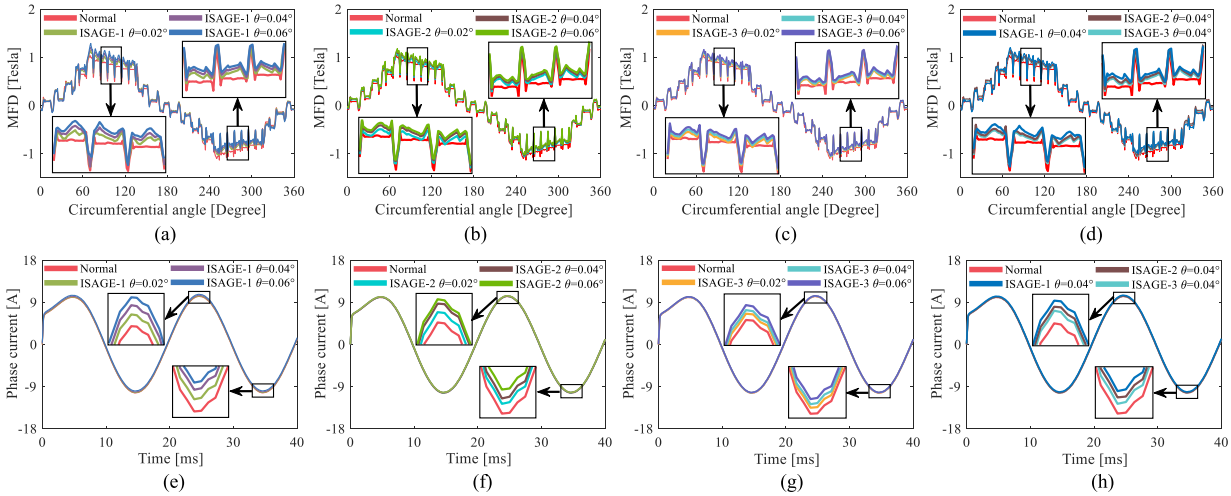

FIGURE 9. MFD in radial section and phase current results in FEA, (a)-(c) MFD results with ISAGE-1 case to ISAGE-3 case, (d) MFD results with different ISAGE case when θ is 0.04°, (e)-(g) phase current results with ISAGE-1 case to ISAGE-3 case, (h) phase current results with different ISAGE case when θ is 0.04°.

eccentricity $g_0\delta_s$ has an equal proportion relation, which brings convenience to the analysis of the paper. Therefore, we take the radial section MFD at 97.5mm (3/4L) on the right side of the left end face of the stator as an example to illustrate the impact of inclined angle on MFD, which is also consistent with Fig. 5. The MFD of different ISAGE cases within this radial section are summarized, as seen in Fig. 9 (a)-(d). When coordinate origin (o) is constant, the amount of amplitude variation of the MFD/phase current will be increased with the development of θ, as shown in Fig. 9 (a)-(c) and (e)-(g). The reason is that the larger the θ, the greater the $g_0\delta_s$ in the same radial section will be. When the inclination angle (θ) is constant, the $g_0\delta_s$ corresponding to the radial section decreases as the coordinate origin (o) moves to the midpoint of stator center axis (ISAGE-1 to ISAGE-3), which will cause the amount of amplitude variation of the MFD /phase current to decrease, but it is still larger than the normal case, as indicated in Fig. 9 (d) and (h). Comparing Fig. 9 (a) & (e) with Fig. 9 (d) & (h), the ISAGE-1 $\theta = 0.06°$ case has the biggest impact on the electromagnetic performance (MFD and phase current) in all cases. This result is good accordance with the theoretical analysis.

The stator MPPUA for 10 ISAGE cases in Table 3 obtained by FEA is shown in Fig. 10. The time domain waves of MPPUA under different ISAGE cases are shown in Fig. 10 (a)-(d). It can be seen that ISAGE will increase the general amplitude of MPPUA. Specifically, the time domain wave of MPPUA is relatively smooth in normal conditions, and there is a sudden change in the wave of ISAGE case. As indicated in Fig. 10 (a), the MPPUA in the ISAGE-1 case has the drastic variation. The unsteady waveform indicates that the stator force subject to MPPUA is not stable, which is prone to induce large vibration. Similarly, with the increase of θ, the amplitude of MPPUA will also be increased, as seen in Fig. 10 (a)-(c). Besides, the largest amplitude of MPPUA in the ISAGE case is ISAGE-1, see Table 4.

The spectrum corresponding to the MPPUA for 10 ISAGE cases are shown in Fig. 10 (e)-(h). The spectrum is mainly

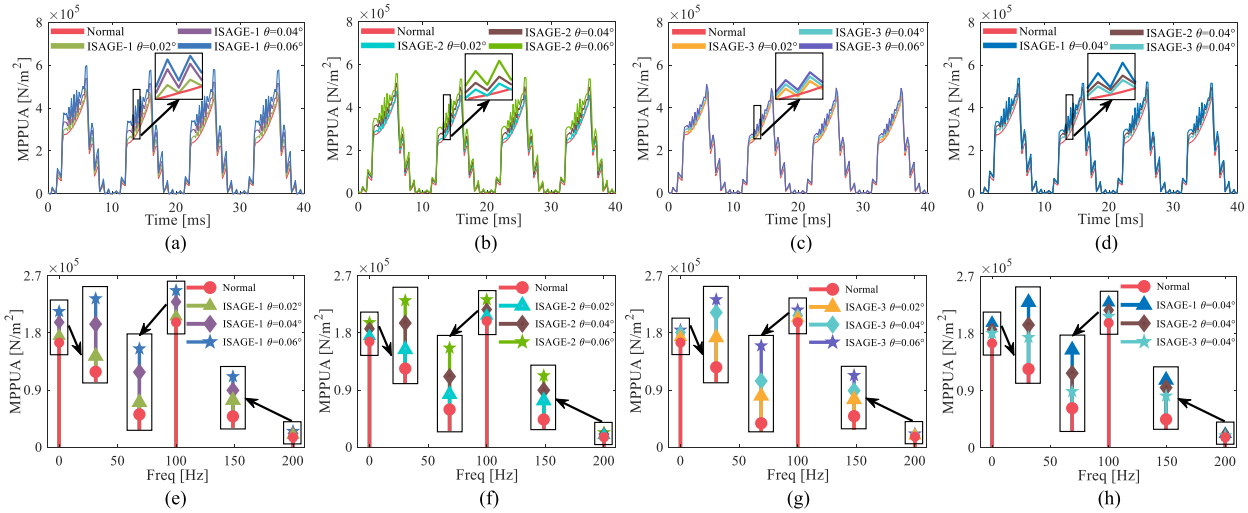

FIGURE 10. Time domain waves and spectra of MPPUA by FEA: (a) and (e) ISAGE-1 cases, (b) and (f) ISAGE-2 cases, (c) and (g) ISAGE-3 cases, (d) and (h) summarize the cases, when θ is 0.04°.

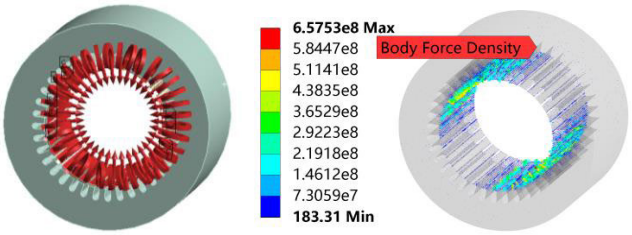

FIGURE 11. Load distribution of different modules, (a) harmonic response module, (b) transient structural module.

constituted by the DC component, 2nd and 4th harmonics. Comparatively, the amplitude of the 4th harmonic is considerably smaller than the DC or 2nd harmonic. With the increase of the inclination angle (θ) in ISAGE, not only the DC component but also the 2nd and 4th harmonics of MPPUA will be increased, as shown in Fig. 10 (e), (f) and (g). Conversely, as the coordinate origin (o) moves to the midpoint of stator center axis (ISAGE-1 to ISAGE-3) when the inclination angle (θ) is constant, the DC component, the 2nd and 4th harmonics of the MPPUA all decrease, as indicated in Fig. 10 (h). This result is consistent with Eq. (12) and Table 1. Among the 10 ISAGE cases, ISAGE-1 θ =0.06 has the largest amplitude of the DC component, 2nd and 4th harmonics. More details can be seen in Table 4.

In this paper, not only the spectrum analysis of MPPUA is carried out, but also the mechanical response and harmonic response of the stator under the action of MPPUA are studied. The excitation loads imported by different modules are shown in Fig. 11.

The mechanical response indicators include vibration, periodic deformation (contraction-expansion movement), strain and stress. Firstly, the vibration acceleration of the stator is analyzed based on the harmonic response module. In order to be consistent with the experiment, the extraction position of vibration data in FEA is the same as the installation position of the acceleration vibration sensor in

TABLE 3. Different cases.

Case	Full name	Case	Full name
1	normal	6	ISAGE-2 θ=0.04°
2	ISAGE-1 θ=0.02°	7	ISAGE-2 θ=0.06°
3	ISAGE-1 θ=0.04°	8	ISAGE-3 θ=0.02°
4	ISAGE-1 θ=0.06°	9	ISAGE-3 θ=0.04°
5	ISAGE-2 θ=0.02°	10	ISAGE-3 θ=0.06°

the experiment. The results of the harmonic response analysis are shown in Figure 12. It can be seen that two peaks of the stator vibration acceleration spectrum are located at the 2nd and 4th harmonics, respectively. What's more, the amplitude of the 2nd harmonic is much larger than the 4th harmonic, which is consistent with the spectrum analysis conclusion of MPPUA. As shown in Fig. 12 (a)-(c), as the inclination angle (θ) increases, the amplitudes of both the 2nd and 4th harmonics of the stator vibration will increase, and the increase of the 2nd harmonic is particularly significant. As shown in Fig. 12 (d), when the inclination angle (θ) is constant, both the 2nd and 4th harmonics of the stator vibration decrease when the coordinate origin (o) moves to the midpoint of stator center axis (ISAGE-1 to ISAGE-3). Similarly, comparing the ISAGE-1 θ = 0.06° case with the other cases, it has an overwhelmingly effect on the stator vibration acceleration in FEA. More details can be seen in Table 4.

Under the action of MPPUA, the stator mechanical response includes deformation, strain and stress, as seen in Fig. 13. The FEA results show that under normal case, the maximum deformation position is located at the left stator tooth tip, as shown in Fig. 13 (a). In addition, the maximum strain position and stress position are located on the inner wall of the slot on the left side of the stator, as shown in Fig. 13 (a). During the ISAGE fault, the position of maximum deformation is still located on the stator tooth tip, but on the right side of the stator, as shown in Fig. 13 (b)-(f). However, the peak value in ISAGE will be larger than the normal case. Similarly, the maximum strain and stress positions are on the inner wall of the tooth slot on the right side of the stator, as shown

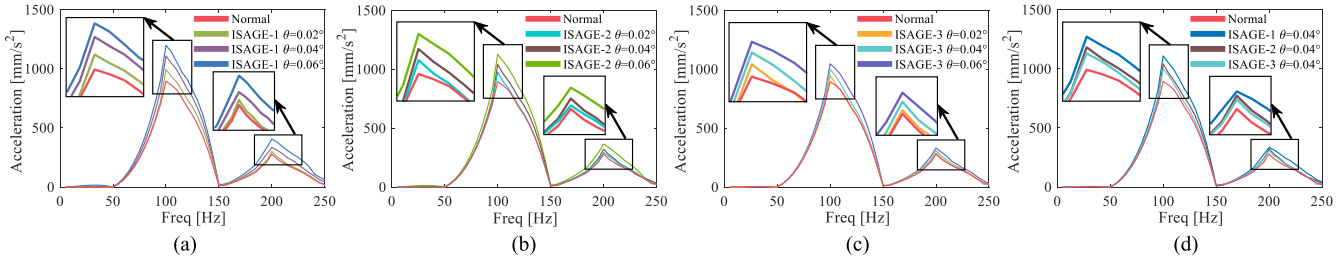

FIGURE 12. Vibration acceleration of stator by FEA, (a) ISAGE-1 cases, (b) ISAGE-2 cases, (c) ISAGE-3 cases, (d) summarize the cases, when θ is 0.04°.

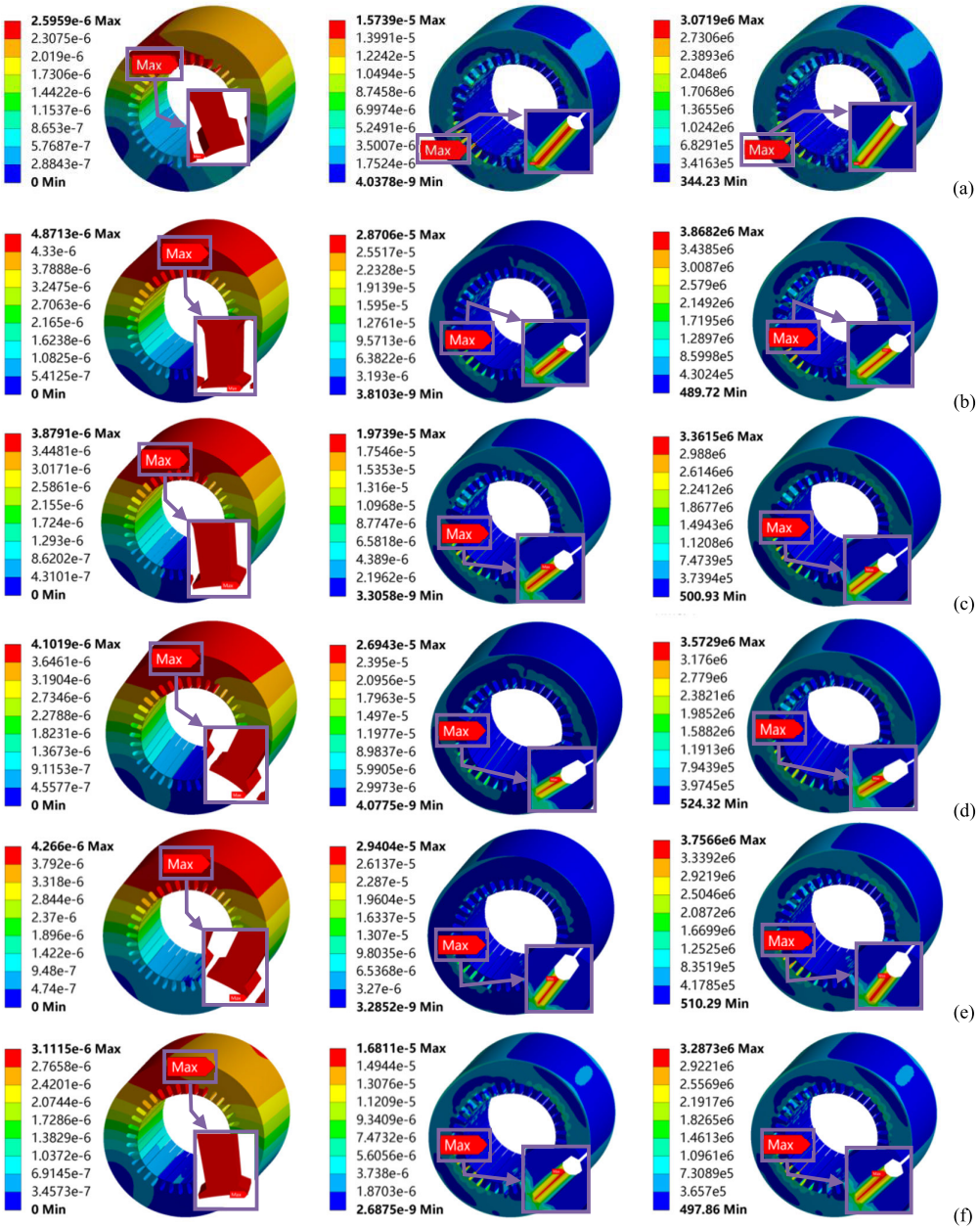

FIGURE 13. Deformation, strain and stress (from left to right) with different cases, (a) normal case, (b) ISAGE-1 case when θ is 0.04°, (c) ISAGE-2 case when θ is 0.02°, (d) ISAGE-2 case when θ is 0.04°, (e) ISAGE-2 case when θ is 0.06°, (f) ISAGE-3 case when θ is 0.04°.

in Fig. 13 (b)-(f). It is worth noting that the deformation of stator tooth tip is a pulsating deformation alternating between contraction and expansion. The increase of deformation in the ISAGE fault will lead to an increase in extrusion and friction between the stator tip and slot wedge, and the wear of the stator tip will increase accordingly. In addition, the

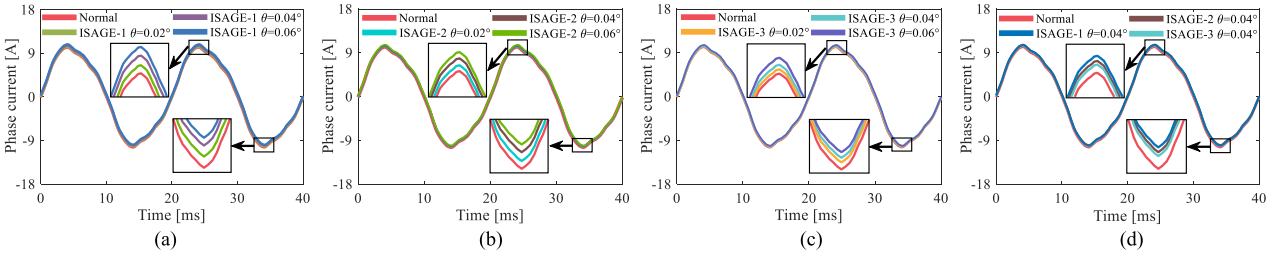

FIGURE 14. Phase current variations in experiment, (a) ISAGE-1 cases, (b) ISAGE-2 cases, (c) ISAGE-3 cases, (d) summarize the cases, when θ is 0.04°.

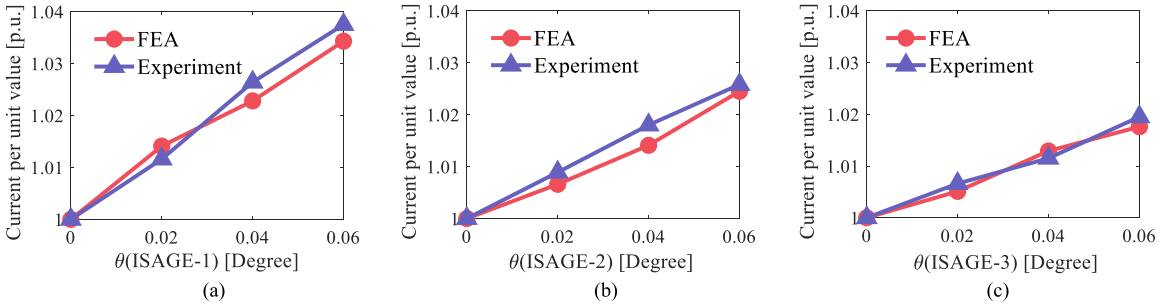

FIGURE 15. Per unit value of phase current amplitude, (a) ISAGE-1 cases, (b) ISAGE-2 cases, (c) ISAGE-3 cases.

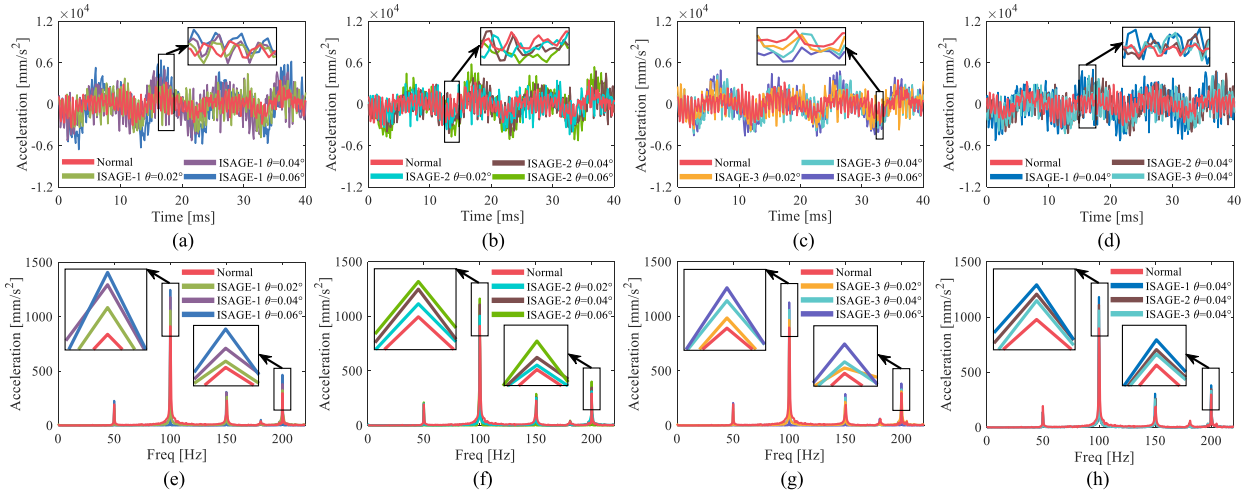

FIGURE 16. Time domain waves and spectra of stator vibration by experiment, (a)-(c) ISAGE-1 cases, ISAGE-2 cases, and ISAGE-3 cases in time domain, respectively, (d) ISAGE-1 to ISAGE-3 in time domain when θ is 0.04°, (e)-(g) ISAGE-1 cases, ISAGE-2 cases, and ISAGE-3 cases in spectra, respectively, (h) ISAGE-1 to ISAGE-3 in spectra when θ is 0.04°.

maximum strain and stress on the inner wall of the slot will be increased in ISAGE fault, and the insulation between stator laminations may be damaged due to the stress concentration effect. Therefore, we can conclude that the probability of failure at tooth tip and inner slot wall will increase.

Furthermore, the bigger the inclined angle (θ), the larger the maximum value of deformation, strain and stress of the stator. On the contrary, the maximum value of deformation, strain and stress of the stator will be decreased as the coordinate origin (o) moves to the midpoint of the stator center axis (ISAGE-1 to ISAGE-3) when the inclination angle (θ) is constant. Importantly, the ISAGE-1 $\theta = 0.06°$ case has the largest value of deformation/strain/stress among the 10 cases. More details can be found in Table 5.

C. EXPERIMENT RESLUTS AND DISCUSSION

It is hard to measure MFD directly due to rotor rotation. Alternatively, we test the phase current to verify the MFD variation in FEA with 10 ISAGE cases, as shown in Fig. 14. For the convenience of comparison, the amplitude changes of phase current in both FEA and experiment in different cases are summarized, as shown in Fig. 15. Although there are some measure errors caused by CT in the experiment, it can be seen that the FEA and experimental results have a small difference. The experiment result well follows the FEA result.

As mentioned before, due to the effect of MPPUA, the stator will vibrate at the same frequency as MPPUA. Therefore, the vibration acceleration of stator can reflect the MPPUA. More details can be seen in Eq. (12). The experimental results of stator vibration before and after ISAGE are shown in

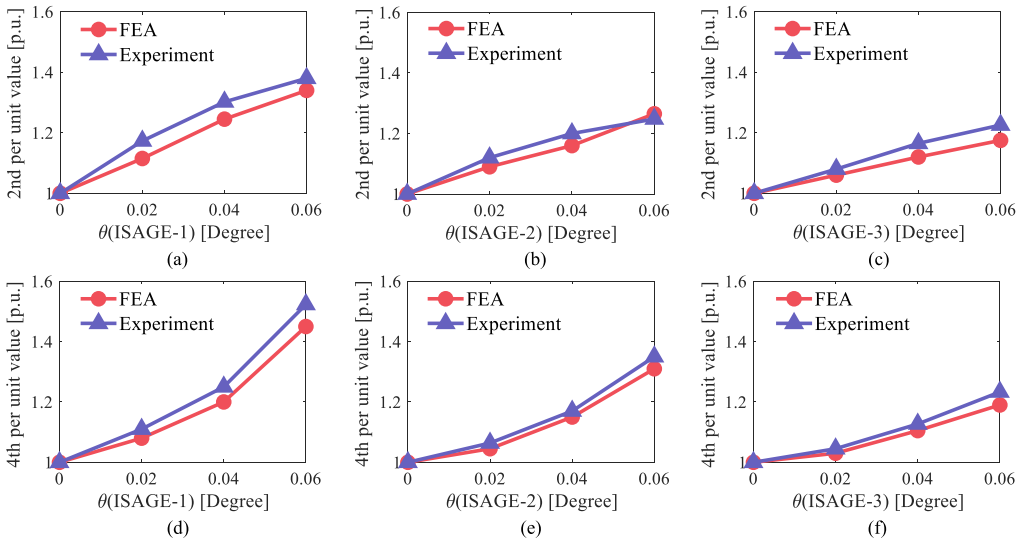

FIGURE 17. Per unit value of 2nd and 4th harmonic, (a) and (d) ISAGE-1 cases, (b) and (e) ISAGE-2 cases, (c) and (f) ISAGE-3 cases.

TABLE 4. Key component amplitudes of MPPUA and stator vibration by FEA.

Case	MPPUA (FEA)						Vibration acceleration (FEA)			
	DC (N/m^2)		2nd (N/m^2)		4th (N/m^2)		2nd (mm/s^2)		4th (mm/s^2)	
Normal	164603.8	1 p.u.	196670.1	1 p.u.	16360.4	1 p.u.	893.4	1 p.u.	279.7	1 p.u.
ISAGE-1 θ=0.02°	180729.8	1.10 p.u.	208700.9	1.06 p.u.	19731.4	1.21 p.u.	993.2	1.11 p.u.	301.5	1.08 p.u.
ISAGE-1 θ=0.04°	193189.1	1.17 p.u.	233505.4	1.19 p.u.	22517.2	1.38 p.u.	1109.5	1.24 p.u.	335.0	1.20 p.u.
ISAGE-1 θ=0.06°	210070.6	1.28 p.u.	251795.6	1.28 p.u.	25969.9	1.59 p.u.	1199.1	1.34 p.u.	405.8	1.45 p.u.
ISAGE-2 θ=0.02°	171568.8	1.04 p.u.	211112.2	1.07 p.u.	19437.0	1.19 p.u.	975.3	1.09 p.u.	292.5	1.05 p.u.
ISAGE-2 θ=0.04°	183067.3	1.11 p.u.	221139.2	1.12 p.u.	21290.2	1.30 p.u.	1040.3	1.16 p.u.	321.9	1.15 p.u.
ISAGE-2 θ=0.06°	192877.2	1.17 p.u.	237166.0	1.21 p.u.	23844.2	1.46 p.u.	1127.4	1.26 p.u.	365.7	1.31 p.u.
ISAGE-3 θ=0.02°	170237.9	1.03 p.u.	207611.9	1.06 p.u.	18923.8	1.16 p.u.	948.4	1.06 p.u.	288.6	1.03 p.u.
ISAGE-3 θ=0.04°	177451.6	1.08 p.u.	211478.2	1.08 p.u.	19938.8	1.22 p.u.	1000.4	1.12 p.u.	309.9	1.11 p.u.
ISAGE-3 θ=0.06°	181196.5	1.10 p.u.	220529.6	1.12 p.u.	21683.5	1.33 p.u.	1046.9	1.17 p.u.	332.2	1.19 p.u.

TABLE 5. Peak value of stator mechanical response by FEA.

Case	Stator mechanical response (FEA)					
	Deformation ($\times10^{-6}$m)		Strain ($\times10^{-5}$)		Stress ($\times10^{6}$Pa)	
Normal	2.60	1 p.u.	1.57	1 p.u.	3.07	1 p.u.
ISAGE-1 θ=0.02°	4.39	1.69 p.u.	2.53	1.61 p.u.	3.64	1.19 p.u.
ISAGE-1 θ=0.04°	4.87	1.87 p.u.	2.87	1.83 p.u.	3.87	1.26 p.u.
ISAGE-1 θ=0.06°	5.18	1.99 p.u.	3.06	1.95 p.u.	4.08	1.33 p.u.
ISAGE-2 θ=0.02°	3.88	1.49 p.u.	1.97	1.25 p.u.	3.36	1.09 p.u.
ISAGE-2 θ=0.04°	4.10	1.58 p.u.	2.69	1.71 p.u.	3.57	1.16 p.u.
ISAGE-2 θ=0.06°	4.27	1.64 p.u.	2.94	1.87 p.u.	3.76	1.22 p.u.
ISAGE-3 θ=0.02°	2.94	1.13 p.u.	1.64	1.04 p.u.	3.21	1.05 p.u.
ISAGE-3 θ=0.04°	3.11	1.20 p.u.	1.68	1.07 p.u.	3.29	1.07 p.u.
ISAGE-3 θ=0.06°	3.42	1.32 p.u.	1.94	1.24 p.u.	3.48	1.13 p.u.

TABLE 6. Key component amplitudes of stator vibration by experiment.

Case	Vibration acceleration (Experiment)			
	2nd (mm/s^2)		4th (mm/s^2)	
Normal	912.8	1 p.u.	291.3	1 p.u.
ISAGE-1 θ=0.02°	1072.9	1.18 p.u.	322.3	1.11 p.u.
ISAGE-1 θ=0.04°	1196.6	1.31 p.u.	364.7	1.25 p.u.
ISAGE-1 θ=0.06°	1263.9	1.38 p.u.	447.4	1.54 p.u.
ISAGE-2 θ=0.02°	1019.4	1.12 p.u.	307.6	1.06 p.u.
ISAGE-2 θ=0.04°	1093.5	1.20 p.u.	341.0	1.17 p.u.
ISAGE-2 θ=0.06°	1142.4	1.25 p.u.	394.5	1.35 p.u.
ISAGE-3 θ=0.02°	983.7	1.08 p.u.	301.6	1.04 p.u.
ISAGE-3 θ=0.04°	1063.4	1.17 p.u.	325.5	1.12 p.u.
ISAGE-3 θ=0.06°	1124.0	1.23 p.u.	357.6	1.23 p.u.

Fig. 16. As shown in Fig. 16 (a)-(c), the peak-to-peak value (passband amplitude) of the stator vibration will be enlarged significantly with increase of θ. At the same time, the 2nd and 4th harmonics will also be increased in ISAGE, as shown in Fig. 16 (e)-(g). When the inclination angle (θ) is constant, the amplitude of each frequency component in ISAGE-1 is greater than in ISAGE-2 or ISAGE-3, as indicated in Fig. 16 (h). Furthermore, the biggest experimental stator vibration amplitudes of the 2nd and 4th harmonics occur in the ISAGE-1 $\theta = 0.06°$ case. This result well follows the FEA and theoretical results. More details can be in Table 6.

Particularly, the stator vibration acceleration for 2nd and 4th harmonics in the FEA and the experiment are compared, respectively, as shown in Fig. 17. In fact, the deviation between the FEA and experimental data is within the acceptable range of engineering. Therefore, it can be concluded that the variation tendency of the experiment and the FEA are consistent with each other, which also verifies the correctness of the FEA model.

IV. CONCLUSION

In this paper, a comprehensive investigation of the electromagnetic characteristics and stator mechanical performances (vibration, deformation, strain and stress) of generators under

ISAGE is proposed, and verified by FEA and experiments. The innovation of this paper lies in two aspects: 1) A universal ISAGE theoretical model of generators is established, and the expressions of MFD and MPPUA of generators in ISAGE cases are derived, which can be used to calculate the electromagnetic performance and stator vibration characteristics of generators in ISAGE. 2) This paper not only studies the effect of rotor inclination angle (θ), but also considers the change of eccentricity along the axial direction on MPPUA. Meanwhile, we also establish a 3D MFD of the generator, which shows the change law of MFD in ISAGE more clearly. The results of the FEA and the experimental data are in good accordance with the theoretical analysis. The following conclusions can be drawn:

1) The MFD is affected by the z-axis coordinate value z and the rotor inclination angle (θ) in ISAGE. With the z increasing, the MFD moves upward as a whole. The larger the θ is, the more significant of MFD change will be.

2) The stator vibrates at the same frequency as the MPPUA. ISAGE mainly increases the DC component, 2nd and 4th harmonics of MPPUA/stator vibration. The greater the rotor inclination angle (θ) is, the larger the amplitude of MPPUA/stator vibration will be. As the intersection (coordinate origin) of the rotor central axis and the stator central axis approaches the midpoint of the stator central axis (ISAGE-1 to ISAGE-3) when the inclination angle (θ) is constant, the MPPUA/stator vibration amplitude will be decreased, and the MPPUA/stator vibration amplitude of ISAGE-1 is the largest.

3) The tip of the stator teeth near the upper casing is in the position of maximum deformation, and the bottom of the tooth slot near the minimum radial air gap is in the position of maximum strain and maximum stress. As the inclination angle (θ) increases, the maximum value of deformation, strain and stress increases. On the contrary, as the coordinate origin (o) moves to the midpoint of the central axis of the stator (ISAGE-1 to ISAGE-3), the maximum value of deformation, strain and stress will be decreased.

REFERENCES

[1] H. Ehya, I. Sadeghi, and J. Faiz, "Online condition monitoring of large synchronous generator under eccentricity fault," in *Proc. 12th IEEE Conf. Ind. Electron. Appl. (ICIEA)*, Siem Reap, Cambodia, Jun. 2017, pp. 19–24.

[2] D.-J. Kim, H.-J. Kim, J.-P. Hong, and C.-J. Park, "Estimation of acoustic noise and vibration in an induction machine considering rotor eccentricity," *IEEE Trans. Magn.*, vol. 50, no. 2, pp. 857–860, Feb. 2014.

[3] M. Babaei, J. Faiz, B. M. Ebrahimi, S. Amini, and J. Nazarzadeh, "A detailed analytical model of a salient-pole synchronous generator under dynamic eccentricity fault," *IEEE Trans. Magn.*, vol. 47, no. 4, pp. 764–771, Apr. 2011.

[4] B. M. Ebrahimi, J. Faiz, and M. J. Roshtkhari, "Static-, dynamic-, and mixed-eccentricity fault diagnoses in permanent-magnet synchronous motors," *IEEE Trans. Ind. Electron.*, vol. 56, no. 11, pp. 4727–4739, Nov. 2009.

[5] B. L. R. Samaga and K. P. Vittal, "Inclined mixed air gap eccentricity detection method for an induction motor," in *Proc. Int. Conf. Adv. Energy Convers. Technol. (ICAECT)*, Manipal, India, Jan. 2014, pp. 37–41.

[6] A. Rahideh and T. Korakianitis, "Analytical open-circuit magnetic field distribution of slotless brushless permanent-magnet machines with rotor eccentricity," *IEEE Trans. Magn.*, vol. 47, no. 12, pp. 4791–4808, Dec. 2011.

[7] W. Tong, S. Li, X. Pan, S. Wu, and R. Tang, "Analytical model for cogging torque calculation in surface-mounted permanent magnet motors with rotor eccentricity and magnet defects," *IEEE Trans. Energy Convers.*, vol. 35, no. 4, pp. 2191–2200, Dec. 2020.

[8] D. G. Dorrell, M. Popescu, and D. M. Ionel, "Unbalanced magnetic pull due to asymmetry and low-level static rotor eccentricity in fractional-slot brushless permanent-magnet motors with surface-magnet and consequent-pole rotors," *IEEE Trans. Magn.*, vol. 46, no. 7, pp. 2675–2685, Jul. 2010.

[9] Y.-L. He, W.-Q. Deng, G.-J. Tang, X.-L. Sheng, and S.-T. Wan, "Impact of different static air-gap eccentricity forms on rotor UMP of turbogenerator," *Math. Problems Eng.*, vol. 2016, pp. 1–13, Sep. 2016.

[10] S. T. Wan and Y. L. He, "Investigation on stator and rotor vibration characteristics of turbo-generator under air-gap eccentricity fault," *Trans. Can. Soc. Mech. Eng.*, vol. 35, no. 2, pp. 161–176, Mar. 2011.

[11] Y.-L. He, M.-X. Xu, W. Zhang, X.-L. Wang, P. Lu, C. Gerada, and D. Gerada, "Impact of stator interturn short circuit position on end winding vibration in synchronous generators," *IEEE Trans. Energy Convers.*, vol. 36, no. 2, pp. 713–724, Jun. 2021.

[12] J. Faiz and S. M. M. Moosavi, "Review of eccentricity fault detection techniques in IMs focusing on DFIG," in *Proc. IEEE 5th Int. Conf. Power Eng., Energy Electr. Drives (POWERENG)*, Riga, Latvia, May 2015, pp. 513–520.

[13] C. Bruzzese and G. Joksimovic, "Harmonic signatures of static eccentricities in the stator voltages and in the rotor current of no-load salient-pole synchronous generators," *IEEE Trans. Ind. Electron.*, vol. 58, no. 5, pp. 1606–1624, May 2011.

[14] Y.-L. He, M.-X. Xu, J. Xiong, Y.-X. Sun, X.-L. Wang, D. Gerada, and G. Vakil, "Effect of 3D unidirectional and hybrid SAGE on electromagnetic torque fluctuation characteristics in synchronous generator," *IEEE Access*, vol. 7, pp. 100813–100823, 2019.

[15] J. Ma, R. Qu, J. Li, and S. Jia, "Structural optimization of a permanent-magnet direct-drive generator considering eccentric electromagnetic force," *IEEE Trans. Magn.*, vol. 51, no. 3, pp. 1–4, Mar. 2015.

[16] H.-C. Jiang, G.-J. Tang, Y.-L. He, K. Sun, W.-J. Li, and L. Cheng, "Effect of static rotor eccentricity on end winding forces and vibration wearing," *Int. J. Rotating Machinery*, vol. 2021, pp. 1–14, Mar. 2021.

[17] I. R. Ciric, F. I. Hantila, M. Maricaru, and S. Marinescu, "Efficient iterative integral technique for computation of fields in electric machines with rotor eccentricity," *IEEE Trans. Magn.*, vol. 48, no. 2, pp. 1015–1018, Feb. 2012.

[18] Y.-L. He, Y.-Y. Zhang, M.-X. Xu, X.-L. Wang, and J. Xiong, "A new hybrid model for electromechanical characteristic analysis under SISC in synchronous generators," *IEEE Trans. Ind. Electron.*, vol. 67, no. 3, pp. 2348–2359, Mar. 2020.

[19] Y. He, W. Zhang, M. Xu, W. Tao, H. Liu, L. Dou, S. Wan, J. Li, and D. Gerada, "Rotor loss and temperature variation under single and combined faults composed of static air-gap eccentricity and rotor inter-turn short circuit in synchronous generators," *IET Electric Power Appl.*, vol. 15, no. 11, pp. 1529–1546, Nov. 2021.

[20] W. Tao, Y. He, H. Lei, W. Zhang, Y. Sun, and T. Wang, "Research on stator-core temperature characteristics under static air-gap eccentricity in turbo-generator," in *Proc. IEEE Int. Conf. Artif. Intell. Inf. Syst. (ICAIIS)*, Dalian, China, Mar. 2020, pp. 637–642.

[21] G. Mirzaeva and K. I. Saad, "Advanced diagnosis of rotor faults and eccentricity in induction motors based on internal flux measurement," *IEEE Trans. Ind. Appl.*, vol. 54, no. 3, pp. 2981–2991, May/Jun. 2018.

[22] G.-J. Tang, Y.-L. He, S.-T. Wan, and L. Xiang, "Investigation on stator vibration characteristics under air-gap eccentricity and rotor short circuit composite faults," *J. Brazilian Soc. Mech. Sci. Eng.*, vol. 36, no. 3, pp. 511–522, May 2014.

[23] Y.-L. He, M.-Q. Ke, F.-L. Wang, G.-J. Tang, and S.-T. Wan, "Effect of static eccentricity and stator inter-turn short circuit composite fault on rotor vibration characteristics of generator," *Trans. Can. Soc. Mech. Eng.*, vol. 39, no. 4, pp. 767–781, Dec. 2015.

[24] M. Zafarani, B. H. Jafari, and B. Akin, "Lateral and torsional vibration monitoring of multistack rotor induction motors," *IEEE Trans. Ind. Electron.*, vol. 68, no. 4, pp. 3494–3505, Apr. 2021.

[25] Y. Akiyama and O. Sugiura, "A study of 2 sf beat phenomena in induction motors," in *Proc. Conf. Rec. IEEE Ind. Appl. Soc. Annu. Meeting*, Houston, TX, USA, Oct. 1992, pp. 100–106.

[26] M. Ojaghi and M. Mohammadi, "Unified modeling technique for axially uniform and nonuniform eccentricity faults in three-phase squirrel cage induction motors," *IEEE Trans. Ind. Electron.*, vol. 65, no. 7, pp. 5292–5301, Jul. 2018.

[27] D. G. Dorrell, "Sources and characteristics of unbalanced magnetic pull in three-phase cage induction motors with axial-varying rotor eccentricity," *IEEE Trans. Ind. Appl.*, vol. 47, no. 1, pp. 12–24, Feb. 2011.
[28] A. Tenhunen, T. Benedetti, T. P. Holopainen, and A. Arkkio, "Electromagnetic forces of the cage rotor in conical whirling motion," *IEE Proc. B Electr. Power Appl.*, vol. 150, no. 5, pp. 563–568, Sep. 2003.
[29] X. Li, Q. Wu, and S. Nandi, "Performance analysis of a three-phase induction machine with inclined static eccentricity," *IEEE Trans. Ind. Appl.*, vol. 43, no. 2, pp. 531–541, Mar. 2007.
[30] X. Wang, Y. He, H. Wang, A. Hu, and X. Zhang, "A novel hybrid approach for damage identification of wind turbine bearing under variable speed condition," *Mechanism Mach. Theory*, vol. 169, Mar. 2022, Art. no. 104629.

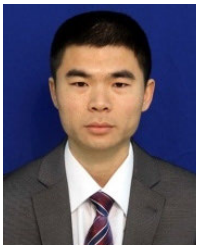

YU-LING HE (Senior Member, IEEE) was born in Longyan, Fujian, China, in 1984. He received the dual B.S. degree in mechanical engineering and electrical engineering, the M.S. degree in mechatronics engineering, and the Ph.D. degree in power machinery and engineering from North China Electric Power University, Baoding, China, in 2007, 2009, and 2012, respectively.

From 2012 to 2015, he was an Assistant Professor of mechatronics engineering with the Department of Mechanical Engineering, North China Electric Power University, where he is currently a Professor and the Head of the Department of Mechatronics Engineering. His research interests include condition monitoring and control on electric machines, signal analysis and processing, testing technology, and mathematical modeling in engineering. He is also an Editorial Member of three international journals, the Hebei Provincial Top Youth Talent, the 3-3-3 Project Talent of Hebei Province, and the Secretary General of Hebei Provincial Society for Vibration Engineering. He was awarded as an Excellent Graduate of Beijing City, from North China Electric Power University, in 2012.

YONG LI (Graduate Student Member, IEEE) was born in Nanchong, Sichuan, China, in 1999. He received the B.S. degree in mechanical engineering from North China Electric Power University, Baoding, China, in 2021, where he is currently pursuing the M.S. degree in mechatronics engineering.

His current research interest includes fault diagnosis on large synchronous generators.

WEN ZHANG (Graduate Student Member, IEEE) was born in Wuhu, Anhui, China, in 1994. He received the B.S. and M.S. degrees in mechanical engineering from North China Electric Power University, Baoding, China, in 2018 and 2021, respectively, where he is currently pursuing the Ph.D. degree in power machinery and engineering.

His current research interests include condition monitoring, fault diagnosis and multi-physics field analysis of large synchronous generators.

MING-XING XU (Graduate Student Member, IEEE) was born in Jiangxi, China, in 1994. He received the B.S. and M.S. degrees in mechanical engineering from North China Electric Power University, Baoding, China, in 2017 and 2020, respectively, where he is currently pursuing the Ph.D. degree in power machinery and engineering.

His research interests include faulty characteristic analysis and monitoring on large synchronous generators.

YI-FAN BAI (Student Member, IEEE) was born in Zhangjiakou, Hebei, China, in 1999. She received the B.S. degree in process equipment and control engineering from the China University of Petroleum, Beijing, in 2021. She is currently pursuing the M.S. degree in mechatronics engineering with North China Electric Power University.

Her current research interest includes fault diagnosis on large synchronous generators.

XIAO-LONG WANG (Member, IEEE) was born in Heilongjiang, China, in 1989. He received the B.S. degree in mechanical engineering and the Ph.D. degree in power machinery and engineering from North China Electric Power University, Baoding, China, in 2011 and 2017, respectively.

He is currently an Assistant Professor with the Department of Mechanical Engineering, North China Electric Power University. His research interests include intelligent fault identification and signal analysis.

SHAN-ZHE SHI was born in Hebei, China, in 1984. He received the B.S. degree, in 2007, and the M.S. degree in electrical engineering from North China Electric Power University, Baoding, China, in 2014. Since 2007, he has been an Engineer with State Grid Hebei Electric Power Company Ltd. His research interest includes property analysis on generator-grid interaction systems.

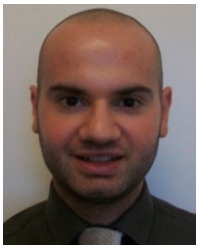

DAVID GERADA (Senior Member, IEEE) received the Ph.D. degree in high-speed electrical machines from the University of Nottingham, Nottingham, U.K., in 2012.

From 2007 to 2016, he was with the Research and Development Department, Cummins Inc. At Cummins, he pioneered the design and development of high-speed electrical machines, transforming a challenging technology into a reliable one suitable for the transportation market, and establishing industry-wide used metrics for such machinery. In 2016, he joined the University of Nottingham, as a Senior Fellow in electrical machines, responsible for developing state of the art electrical machines for future transportation which push existing technology boundaries, while propelling the new technologies to high technology readiness levels (TRL). His research interests include novel materials and applications in electromechanical energy conversion, traction machines, and mechatronics.

Dr. Gerada is a member of the Institution of Engineering and Technology. He is a Chartered Engineer in U.K.